International Journal of Engineering and Advanced Technology (IJEAT)
ISSN: 2249-8958 (Online), Volume-11 Issue-4, April 2022

Relating Mandelbrot and Barnes-Jarvis Power Law Noise State Space Models using Partial Fractions

Naleli Jubert Matjelo, Sekhonyana Moeti, Molise Mokhomo

Abstract*: *This paper addresses two state space models for generating approximate power law noise and shows that these models are related through partial fractions in frequency domain.

Keywords:* *State Space Model, Power Law Noise, Partial Fractions, Mandelbrot Model, Barnes-Jarvis Model.

I. INTRODUCTION

Power law noise is ubiquitous in a wide variety of dynamic systems ranging from electronic oscillators [1], [2], [3], [4], [5], [6] to quantum information processing systems [7], [8], [9] and quantum sensors [10]. For example, the stability of optical atomic clocks [11] is often limited by frequency noise of the laser (local oscillator) used to probe the atomic transition. State-of-the-art cavity-stabilized lasers are limited by thermomechanical noise with a flicker power law spectrum [12]. In general, the instabilities of most oscillators can be modeled by a combination of power-law noise types having a power spectral density (PSD) $S_y(f) \propto f^{\lambda}$ where f is the noise frequency in Hz and λ is a constant defining the PSD slope. Table 1 below shows some of these power law noise types.

TABLE 1: POWER LAW NOISE TYPES [13]

Noise Type	Exponent λ	PSD $S_y(f)$
White PM	2	-
Flicker PM	1	$h_1 sinc^2(\pi f \tau)$
White FM	0	$h_0 f^{-0}$
Flicker	-1	$h_{-1} f^{-1}$
Random Walk FM	-2	$h_{-2} f^{-2}$
Flicker Walk	-3	$h_{-3} f^{-3}$
Random Run	-4	$h_{-4} f^{-4}$

In the field of quantum information processing a central challenge is the detailed understanding and mitigation of decoherence inducing noise processes. Methods for mitigation include hardware optimization [14] and noise filtering through control methods [15]. Here too, dominant noise sources are often power law in character either due to fluctuating background fields [16] or in very well isolated systems due to the fundamental instability of the controller's clock reference. As such detailed characterization [17] and modeling [18] of noise processes is crucial to further progress. Measurement and control of dynamic systems exhibiting power law noise using the smoothing, filtering and prediction algorithms of modern control and machine learning often requires identification and state-space modeling of their noise. There are various techniques for modeling approximate power law noise, with most techniques involving filtering of white noise in either the Fourier [19] or state-space domain. In this paper we provide a tutorial description of two well-known state-space models for modeling approximate power law noise: the Mandelbrot model, which is simply a linear aggregation of first order low pass filters [20], [21] and the Barnes-Jarvis model, which is formed by a cascade of first order filters [22], [23]. We show that these two models are related through a partial fractions transformation and unify their description using a common mathematical framework. This paper proceeds as follows. In the Section II we present the model for a general power law noise and show the transformation from Barnes-Jarvis model to Mandelbrot model using partial fractions. Section III concludes this paper with some remarks and possible future work, and the Appendix provides some derivations.

II. POWER LAW NOISE MODELS

A. Overview

We adopt the frequency domain approach presented in [22] for constructing power law noise generation model. Consider a transfer function $G(s)$ made up of cascade of first order filters as shown below,

$$G(s) = \prod_{i=0}^{m-1} G_i(s) = \prod_{i=0}^{m-1} \frac{\tau s + \beta^i}{\alpha\tau s + \beta^i} \qquad (1)$$

where s is the Laplace parameter, $\frac{\beta^i}{\tau}$ is the i^{th} stage zero and $\frac{\beta^i}{\alpha\tau}$ is the i^{th} stage pole with $\beta > 1$. For each stage it is obvious that the low frequency (DC) gain is unity ($\lim_{s\to 0} G_i(s) = 1$) while the high frequency gain is α^{-1}, ($\lim_{s\to\infty} G_i(s) = \alpha^{-1}$). That means a single stage changes the magnitude of the transfer function by a factor α^{-1}. It is clear then that for an m-stage cascade the magnitude of $G(s)$ changes by a factor α^{-m} in the frequency range $[\frac{\beta^0}{2\pi\tau}, \frac{\beta^m}{2\pi\tau}]$.

Manuscript received on 22 March 2022
Revised Manuscript received on 31 March 2022
Manuscript published on 30 April 2022
* Correspondence Author
Naleli Jubert Matjelo*, Department of Physics and Electronics, National University of Lesotho (NUL), Roma, Lesotho. Email: nj.matjelo@nul.ls
Sekhonyana Moeti, Department of Engineering, Minopex Lesotho Pty (LTD), Mokhotlong, Lesotho. Email: moeti.sekhonyana@gmail.com
Molise Mokhomo, Mukuru, Cape Town, Western Cape, South Africa. Email: mmokhomo@gmail.com

The power spectral density $S_y(s)$ of a power law noise has the following general form,

$$S_y(s) = A^2|s|^{\lambda} \tag{2}$$

where A is a constant, $\lambda \in [2, 4]$, i.e. for flicker noise $\lambda = -1$. To mimic this power spectral density the following condition must hold [22],

$$\left|\frac{S_y\left(\frac{j\beta^m}{\tau}\right)}{S_y\left(\frac{j\beta^0}{\tau}\right)}\right| = \left|\frac{\beta^m}{\beta^0}\right|^{\lambda} = \beta^{m\lambda} \approx \left|\frac{G\left(\frac{j\beta^m}{\tau}\right)}{G\left(\frac{j\beta^0}{\tau}\right)}\right|^2 = \alpha^{-2m} \tag{3}$$

Thus,

$$\beta \approx \alpha^{-\frac{2}{\lambda}} \tag{4}$$

It should be noted that while β^m controls the band of frequencies (i.e. bandwidth) over which the model approximation is valid, τ controls where this band of frequencies begins and ends (or centered). This means a fixed bandwidth of β^m can be shifted back and forth on the frequency line by simply varying τ. Next we consider two state space models derived from this general cascade transfer function model. For simulation purposes we need to pick a value, or a few, for λ and here we choose $\lambda = -1$ from now onward, without loss of generality.

B. Barnes-Jarvis State Space Model

In this section we consider a cascade model from the previous section and show its Bode diagram and power spectral density, which falls approximately as $1/f$ over a frequency interval dictated by the choice of τ and β^m. The transfer function $G(s)$ for this cascade model is shown below,

$$G(s) = \prod_{i=0}^{m-1} \frac{\tau s + \beta^i}{\alpha\tau s + \beta^i} \tag{5}$$

Fig. 1 below shows the Bode plot of this transfer function together with its constituent cascade stages for settings $m = 4, \lambda = -1, \tau = 500s, \alpha = 3$ and $\beta = 9$.

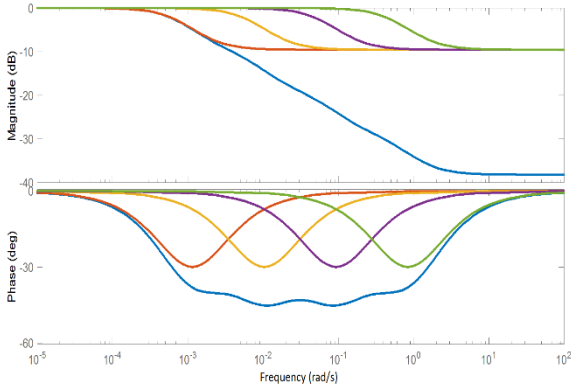

Fig. 1. Bode diagram for Barnes-Jarvis cascade model

The Bode diagram paints a picture of how individual frequency-shifted low pass filter stages contribute to the overall appearance of a $1/f$ fall-off. Fig. 2 below shows the log-log plot of the above model superimposed on the exact/expected flicker noise spectral plot slope.

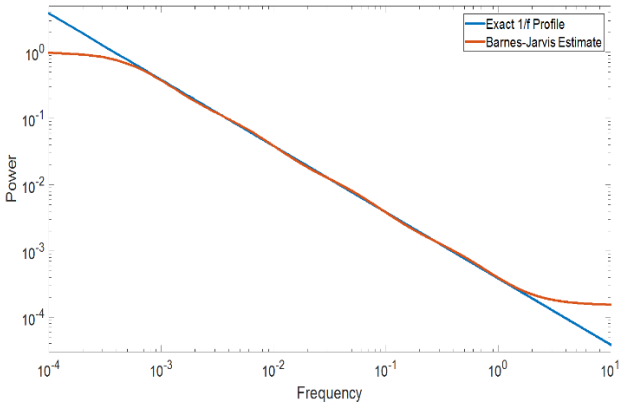

Fig. 2. Barnes-Jarvis model power spectral density fit.

Given the desired approximation accuracy, the parameters τ and β^m can be adjusted until the acceptable approximation error is obtained to within the desired range of frequencies by making reference to the power spectral density plot in Fig. 2 above. One way to convert the above transfer function to state space is by converting each cascade stage into state space and augment the resulting state space models by noting that the output of one stage becomes the input to the next stage. Following this line of thinking the resulting continuous-time state space is as follows,

$$\begin{aligned} \dot{\boldsymbol{z}} &= \boldsymbol{A_c z} + \boldsymbol{B_c} r \\ w &= \boldsymbol{C^T z} + \boldsymbol{D} r \end{aligned} \tag{6}$$

where r is the input white noise, w is the estimated output flicker noise, $\boldsymbol{z}$ is the state vector and the continuous-time matrices $\boldsymbol{A_c}$, $\boldsymbol{B_c}$, $\mathbf{C}$ and $\mathbf{D}$ for model size $m = 4$ are given by,

$$\begin{aligned} \boldsymbol{A}_c &= \begin{bmatrix} \frac{-\beta^0}{\alpha\tau} & 0 & 0 & 0 \\ \frac{(\alpha-1)\beta^0}{\alpha^2\tau} & \frac{-\beta^1}{\alpha\tau} & 0 & 0 \\ \frac{(\alpha-1)\beta^0}{\alpha^3\tau} & \frac{(\alpha-1)\beta^1}{\alpha^2\tau} & \frac{-\beta^2}{\alpha\tau} & 0 \\ \frac{(\alpha-1)\beta^0}{\alpha^4\tau} & \frac{(\alpha-1)\beta^1}{\alpha^3\tau} & \frac{(\alpha-1)\beta^2}{\alpha^2\tau} & \frac{-\beta^3}{\alpha\tau} \end{bmatrix} \\ \boldsymbol{B}_c^T &= \begin{bmatrix} \frac{1}{\alpha^1\tau} & \frac{1}{\alpha^2\tau} & \frac{1}{\alpha^3\tau} & \frac{1}{\alpha^4\tau} \end{bmatrix} \\ \boldsymbol{C}^T &= (\alpha-1)\begin{bmatrix} \frac{\beta^0}{\alpha^4} & \frac{\beta^1}{\alpha^3} & \frac{\beta^2}{\alpha^2} & \frac{\beta^3}{\alpha^1} \end{bmatrix} \\ \boldsymbol{D} &= \begin{bmatrix} \frac{1}{\alpha^4} \end{bmatrix} \end{aligned} \tag{7}$$

The details of this conversion above can be found in the Appendix. The corresponding discrete-time state space model has the following form,

$$\begin{aligned} \boldsymbol{z}_{k+1} &= \boldsymbol{A z}_k + \boldsymbol{B} r_k \\ w_k &= \boldsymbol{C^T z}_k + \boldsymbol{D} r_k \end{aligned} \tag{8}$$

where k represents the k^{th} time instance at time $t = kT$ for some sampling period T and the discrete-time matrices are given by,

$$\boldsymbol{A} = e^{\boldsymbol{A}_c T}$$
$$\boldsymbol{B} = \boldsymbol{A}_c^{-1}(e^{\boldsymbol{A}_c T} - \boldsymbol{I})\boldsymbol{B}_c \quad (9)$$

Fig. 3 below shows the PSD plot of a flicker noise data (as reference) and the above Barnes-Jarvis discrete-time state space model simulation output with; $T = 12ms, m = 4, \lambda = -1, \tau = 500s, \alpha = 3$ and $\beta = 9$.

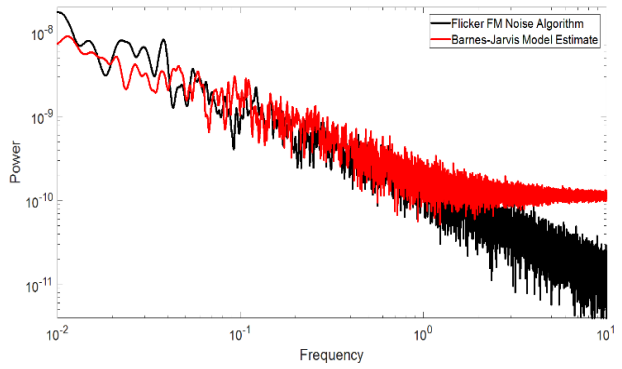

Fig. 3. Barnes-Jarvis discrete-time state space model simulation.

In Fig. 3 above it can be seen that Barnes-Jarvis model is approximating the flicker noise reasonably well for the first two decades and starts to flatten out afterwards thus indicating that the Gaussian white noise is taking over the lead. This is also around the same frequency where our model seemed to deviate from the expected flicker noise slope in Fig. 1 and Fig. 2. From calculations this model should approximate well in the frequency range $\left[\frac{\beta^0}{2\pi\tau}, \frac{\beta^m}{2\pi\tau}\right] = [0.32mHz, 2.09Hz]$.

C. Mandelbrot State Space Model

For the same dynamic process there exist many state space representations which can be transformed from one to another through some appropriate linear transforms. In the previous section we presented the state space model with a lower triangular transition matrix $\boldsymbol{A_c}$ as a consequence of deriving state space directly from Barnes- Jarvis cascade filter model. This transition matrix may not be favorable compared to diagonal transition matrix not just for complicating discretization but also for invoking coupling among state components which may be preferable if they were identically independent for some probability distribution estimations. In this section we transform the Barnes-Jarvis cascade filter approach into a linear combination of low pass filters, which resembles Mandelbrot-like model presented in [20]. This approach will yield a diagonal state transition matrix. We consider again the transfer function $G(s)$ as given in equation (5) and argue that the constituent cascade stages can be represented as a linear combination of corresponding low pass filters with the help of partial fractions. The resulting equivalent transfer function is of the following form,

$$G(s) = \prod_{i=0}^{m-1} \frac{\tau s + \beta^i}{\alpha\tau s + \beta^i} = \sum_{i=0}^{m-1} \frac{\gamma_i}{\alpha\beta^j - \beta^i} + \sum_{i=0}^{m-1} \frac{\gamma_i}{\alpha\tau s - \beta^i} \quad (10)$$

where γ^i is given by,

$$\gamma^i = \frac{(\alpha-1)\beta^i}{\alpha^m} \prod_{\substack{j=0 \\ i\neq j}}^{m-1} \frac{\alpha\beta^j - \beta^i}{\beta^j - \beta^i} \quad (11)$$

The details of partial fractions procedure for the above model can be found in the Appendix. Fig. 4 below shows the Bode plot of this transfer function together with its constituent low pass filters for settings $m = 4, \lambda = -1, \tau = 500s, \alpha = 3$ and $\beta = 9$.

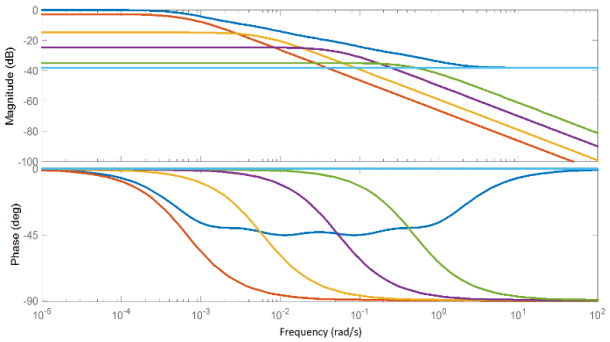

Fig. 4. Bode diagram for Mandelbrot model.

Fig. 5 below shows the log-log plot of the above model superimposed on the exact/expected flicker noise spectral plot.

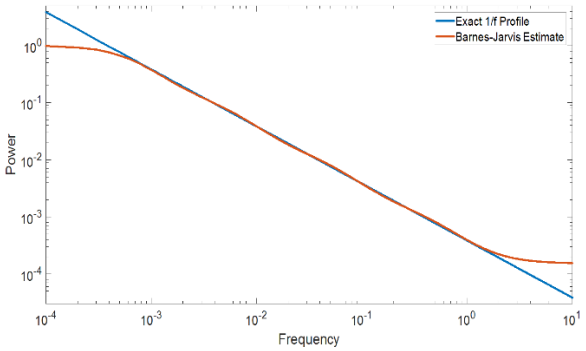

Fig. 5. Mandelbort model power spectral density fit.

Converting the above transfer function to state space is pretty straight forward. We need only convert one low pass filter and copy the procedure to the rest of the low pass filters. The resulting continuous-time state space model has the following form,

$$\dot{\boldsymbol{z}} = \boldsymbol{A_c z} + \boldsymbol{B_c} r$$
$$\mathrm{w} = \mathbf{C^T z} + \mathbf{D}\mathrm{r} \quad (12)$$

where the continuous-time matrices for model size $m = 4$ are as follows,

$$\mathbf{A_c} = \frac{-1}{\alpha\tau} diag([\beta^0 \quad \beta^1 \quad \beta^2 \quad \beta^3])$$
$$\mathbf{B_c^T} = \frac{1}{\alpha\tau}[1 \quad 1 \quad 1 \quad 1]$$
$$\mathbf{C^T} = [\gamma_0 \quad \gamma_1 \quad \gamma_2 \quad \gamma_3] \quad (13)$$
$$\mathbf{D} = \sum_{j=0}^{3} \frac{\gamma_j}{\alpha\beta^i - \beta^j}$$

The details of this conversion above can be found in the Appendix. The discretization procedure is the same as done with the Barnes-Jarvis model in the previous section and yields,

Published By:
Blue Eyes Intelligence Engineering
and Sciences Publication (BEIESP)

$$\boldsymbol{z_{k+1}} = \boldsymbol{Az_k} + \boldsymbol{Br}_k$$
$$\boldsymbol{s}_k = \boldsymbol{C^T z_k} + \boldsymbol{Dr_k} \tag{14}$$

The corresponding discrete-time Mandelbort model matrices are given by,

$$\mathbf{A} = diag\left(\left[e^{\frac{-\beta^0 T}{\alpha\tau}} \quad e^{\frac{-\beta^1 T}{\alpha\tau}} \quad e^{\frac{-\beta^2 T}{\alpha\tau}} \quad e^{\frac{-\beta^3 T}{\alpha\tau}}\right]\right)$$
$$\mathbf{B^T} = \left[\frac{1-e^{\frac{-\beta^0 T}{\alpha\tau}}}{\beta^0} \quad \frac{1-e^{\frac{-\beta^1 T}{\alpha\tau}}}{\beta^1} \quad \frac{1-e^{\frac{-\beta^2 T}{\alpha\tau}}}{\beta^2} \quad \frac{1-e^{\frac{-\beta^3 T}{\alpha\tau}}}{\beta^3}\right] \tag{15}$$
$$\mathbf{C^T} = [\gamma_0 \quad \gamma_1 \quad \gamma_2 \quad \gamma_3]$$
$$\mathbf{D} = \sum_{j=0}^{3} \frac{\gamma_j}{\alpha\beta^i - \beta^j}$$

An emphasis can be made on the discrete-time input matrix $\boldsymbol{B}$ that for it to be evaluated precisely, the continuous-time state transition matrix $\boldsymbol{A_c}$ needs to be full rank (non-singular). In the case whereby $\boldsymbol{A_c}$ is singular the first order Euler methods would suffice as approximate discrete models and the discrete-time state transition and input matrices would simply be $\boldsymbol{A} = \boldsymbol{I} + \boldsymbol{A_c}T$ and $\boldsymbol{B} = \boldsymbol{B_c}T$, respectively. Fig. 6 below shows the simulation of the corresponding discrete-time state space model with $T = 2s,\ \lambda = -1, \tau = 500s, \alpha = 3, \beta = 9$ and γ_i as given in equation (11).

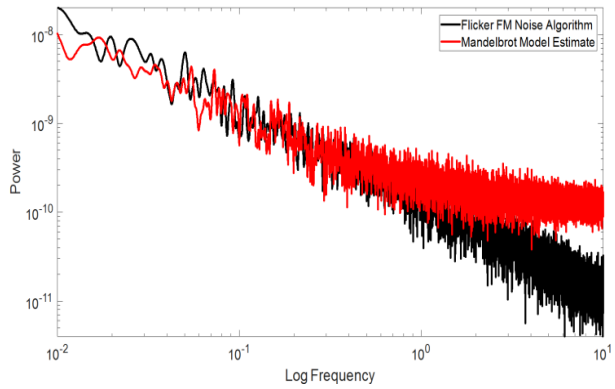

Fig. 6. Mandelbort discrete-time state space model simulation.

Just like with the Barnes-Jarvis there is a deviation from the expected slope after the first two decades. The approximation frequency range is the same as that of Barnes-Jarvis because the two models are related by a linear transformation.

III. ACKNOWLEDGEMENTS AND FUNDING DECLARATION

We declare here that the content in this manuscript is our own unaided contribution/work and the sources used have been well-referenced. There is no one else who contributed to this work. This work is not associated with any funding agency/institution and whichever payable fees relating to this work will be coming from my own pocket.

IV. CONCLUSION

In this paper we presented Barnes-Jarvis and Mandelbrot state space models for generating power law noise in a linear time-invariant fashion. We also demonstrated a partial fraction-based transformation from Barnes-Jarvis cascaded transfer function model to Mandelbrot transfer function model under the assumption of a common/single input Gaussian noise source. These models gave us a way of approximating the power law noise in terms of components of well-known Gaussian white noise such that the precision of the approximation is dependent on the number of Gaussian white noise components used in the model, which is the model size. This way of representing the power law noise in terms of a mixture of Gaussian noise components allows us to adopt the Gaussian mixture models as the framework for estimating and keeping track of the probability distributions associated with power law noise. In future work we wish to demonstrate Bayesian estimation applied on a linear time-invariant process which has power law noise associated with both process dynamics and observation.

V. APPENDIX

A. Barnes-Jarvis State Space Derivation

The cascaded transfer function model in equation (5) can be converted from frequency domain to time domain by considering the idea that the output of one stage becomes an input to the next stage. This means we only convert the individual stages and connect the results together. The individual i^{th} stage, relating the input $R_i(s)$ and $Y_i(s)$, is converted as follows into the corresponding differential equation:

$$\frac{Y_i(s)}{R_i(s)} = \frac{\tau s + \beta^i}{\alpha\tau s + \beta^i} \frac{Z_i(s)}{Z_i(s)} \tag{16}$$

where $Z_i(s)$ represents the i^{th} internal state of the model. Separating the numerators and denominators into separate equations and distributing the internal state throughout we get the following,

$$R_i(s) = \alpha\tau s Z_i(s) + \beta^i Z_i(s) \tag{17}$$
$$Y_i(s) = \tau s Z_i(s) + \beta^i Z_i(s) \tag{18}$$

Taking the Laplace inverse we get the following state space model for the i^{th} cascade stage,

$$r_i(t) = \alpha\tau\dot{z}_i(t) + \beta^i z_i(t) \tag{19}$$
$$y_i(t) = \tau\dot{z}_i(t) + \beta^i z_i(t) \tag{20}$$

Rearranging terms and making substitutions we get,

$$\dot{z}_i(t) = \frac{-\beta^i}{\alpha\tau} z_i(t) + \frac{1}{\alpha\tau} r_i(t) \tag{21}$$
$$y_i(t) = \frac{(\alpha-1)\beta^i}{\alpha} z_i(t) + \frac{1}{\alpha} r_i(t) \tag{22}$$

Now connecting cascade stages means $r_i(t) = y_{i-1}(t)$ and $r_{i+1}(t) = y_i(t)$. From now on we drop off the arguments for convenience. This connection procedure leads to the following coupled differential equations for a model of size m,

$$\dot{z}_0 = -\frac{1}{\alpha\tau}z_0 + \frac{1}{\alpha\tau}r_0 \tag{23}$$

$$\dot{z}_1 = \frac{(\alpha-1)}{\alpha^2\tau}z_0 - \frac{\beta}{\alpha\tau}z_1 + \frac{1}{\alpha^2\tau}r_0 \tag{24}$$

$$\dot{z}_2 = \frac{(\alpha-1)}{\alpha^3\tau}z_0 + \frac{(\alpha-1)\beta}{\alpha^2\tau}z_1 - \frac{\beta^2}{\alpha\tau}z_2 + \frac{1}{\alpha^3\tau}r_0 \tag{25}$$

$$\vdots \tag{26}$$

$$\dot{z}_{m-1} = \frac{(\alpha-1)}{\alpha^m\tau}z_0 + \frac{(\alpha-1)\beta}{\alpha^{m-1}\tau}z_1 + \cdots + \frac{(\alpha-1)\beta^{m-2}}{\alpha^2\tau}z_{m-2} - \frac{\beta^{m-1}}{\alpha\tau}z_{m-1} + \frac{1}{\alpha^m\tau}r_0 \tag{27}$$

$$y_{m-1} = \frac{(\alpha-1)}{\alpha^m}z_0 + \frac{(\alpha-1)\beta}{\alpha^{m-1}}z_1 + \cdots\frac{(\alpha-1)\beta^{m-1}}{\alpha}z_{m-2} + \frac{1}{\alpha^m}r_0 \tag{28}$$

From here we can present everything in a compact matrix formalism by considering a state vector $\boldsymbol{z} = [z_0 \quad z_1 \quad \cdots \quad z_{m-1}]$ and we get the following compact form of state space model,

$$\dot{\boldsymbol{z}} = \boldsymbol{A_c z} + \boldsymbol{B_c} r_0$$
$$y_{m-1} = \boldsymbol{C^T z} + \boldsymbol{D} r_0 \tag{29}$$

and the matrices are made up of the coefficients in the coupled differential equations above as shown below,

$$\boldsymbol{A_c} = \begin{bmatrix} -\frac{\beta^0}{\alpha^1\tau} & 0 & \cdots & 0 & 0 \\ \frac{(\alpha-1)\beta^0}{\alpha^2\tau} & -\frac{\beta^1}{\alpha^1\tau} & \cdots & 0 & 0 \\ \vdots & \vdots & \ddots & \vdots & \vdots \\ \frac{(\alpha-1)\beta^0}{\alpha^{m-1}\tau} & \frac{(\alpha-1)\beta^1}{\alpha^{m-2}\tau} & \cdots & -\frac{\beta^{m-2}}{\alpha^1\tau} & 0 \\ \frac{(\alpha-1)\beta^0}{\alpha^m\tau} & \frac{(\alpha-1)\beta^1}{\alpha^{m-1}\tau} & \cdots & \frac{(\alpha-1)\beta^{m-2}}{\alpha^2\tau} & -\frac{\beta^{m-1}}{\alpha^1\tau} \end{bmatrix} \tag{30}$$

$$\boldsymbol{B_c^T} = \begin{bmatrix} \frac{1}{\alpha^1\tau} & \frac{1}{\alpha^2\tau} & \cdots & \frac{1}{\alpha^m\tau} \end{bmatrix}$$
$$\boldsymbol{C^T} = \begin{bmatrix} \frac{(\alpha-1)\beta^0}{\alpha^m\tau} & \frac{(\alpha-1)\beta^1}{\alpha^m - 1\tau} & \cdots & \frac{(\alpha-1)\beta^{m-1}}{\alpha^1\tau} \end{bmatrix}$$
$$\boldsymbol{D} = \begin{bmatrix} \frac{1}{\alpha^m} \end{bmatrix}$$

B. Partial Fractions

The transfer function from Barnes-Jarvis model, equation (5), has the same degree in the numerator and denominator. However before performing partial fractions decomposition the numerator polynomial must be at least one degree less than the denominator. This can be achieved by carrying out the long division which results in a constant quotient K and the remainder polynomial with at least one degree less than the divisor (denominator) polynomial as shown below,

$$\prod_{i=0}^{m-1}\frac{\tau s+\beta^i}{\alpha\tau s+\beta^i} = K + \sum_{i=0}^{m-1}\frac{\gamma_i}{\alpha\tau s+\beta^i} \tag{31}$$

with the unknowns s, i and K. To find i we simply multiply the above equation by the denominator $\alpha\tau s+\beta^i$ corresponding to i and substitute the pole $s=-\beta^i/\alpha\tau$ throughout as shown below,

$$(\alpha\tau s+\beta^i)\prod_{j=0}^{m-1}\frac{\tau s+\beta^i}{\alpha\tau s+\beta^j}\Big|_{s=\frac{-\beta^i}{\alpha\tau}} = \gamma_i \tag{32}$$

The right-hand side leave γ_i since the rest of the terms are effectively multiplied by zero. Simplifying the left-hand side and rearranging terms we arrive at,

$$\gamma^i = \frac{(\alpha-1)\beta^i}{\alpha^m}\prod_{\substack{j=0\\ i\neq j}}^{m-1}\frac{\alpha\beta^j-\beta^i}{\beta^j-\beta^i} \tag{33}$$

To find K we just choose any of the numerator factor $\tau s+\beta^i$ and substitute its root $s=-\beta^i/\tau$ throughout. This forces the left-hand side of equation (31) to be zero so that we can express K as follows,

$$K = -\sum_{j=0}^{m-1}\frac{\tau s+\beta^i}{\alpha\tau s+\beta^j}\Big|_{s=\frac{-\beta^i}{\alpha\tau}} \tag{34}$$

$$= \sum_{j=0}^{m-1}\frac{\gamma_j}{\alpha\beta^i-\beta^j} \tag{35}$$

C. Mandelbort State Space Derivation

To convert the i^{th} component of the Mandelbrot transfer function, equation (10), from frequency to time domain we follow the same procedure shown with Barnes-Jarvis cascade stage. The i^{th} low pass filter component lead to the following,

$$\frac{Y_i(s)}{R_i(s)} = \frac{\gamma_i}{\alpha\tau s+\beta^i}\frac{Z_i(s)}{Z_i(s)} \tag{36}$$

which gives rise to the following state space model,

$$\dot{z}_i(t) = \frac{\gamma_i}{\alpha\tau}z_i(t) + \frac{1}{\alpha\tau}r_i(t) \tag{37}$$

$$y_i(t) = \gamma_i z_i(t) \tag{38}$$

The constant K gives $y_m(t) = Kr_m(t)$. In this case the internal states $z_i(t)$ are not coupled and the output $y_M(t)$ is given by the sum of all component outputs $y_i(t)$. The resulting equations are as shown below,

$$\dot{z}_0 = -\frac{\beta^0}{\alpha\tau}z_0 + \frac{1}{\alpha\tau}r_0 \tag{39}$$

$$\dot{z}_1 = -\frac{\beta^1}{\alpha\tau}z_1 + \frac{1}{\alpha\tau}r_1 \tag{40}$$

$$\dot{z}_2 = -\frac{\beta^2}{\alpha\tau}z_2 + \frac{1}{\alpha\tau}r_2 \tag{41}$$

Published By:
Blue Eyes Intelligence Engineering
and Sciences Publication (BEIESP)

$$\vdots \tag{42}$$

$$\dot{z}_{m-1} = -\frac{\beta^{m-1}}{\alpha\tau} z_{m-1} + \frac{1}{\alpha\tau} r_{m-1} \tag{43}$$

$$y_M = \gamma_0 z_0 + \gamma_1 z_1 + \cdots + \gamma_{m-1} z_{m-1} + K r_m \tag{44}$$

In compact form with state vector $\boldsymbol{z} = [z_0 \quad z_1 \quad \dots \quad z_{m-1}]^T$ and input vector $\boldsymbol{r} = [r_0 \quad r_1 \quad \dots \quad r_{m-1}]^T$ we get the following,

$$\dot{\boldsymbol{z}} = \boldsymbol{A_c z} + \boldsymbol{B_c r} \tag{45}$$

$$y_M = \boldsymbol{C^T z} + \boldsymbol{D} r_m \tag{46}$$

where the matrices are given by,

$$\begin{aligned} \mathbf{A_c} &= \frac{-1}{\alpha\tau} diag([\beta^0 \quad \beta^1 \quad \dots \quad \beta^{m-1}]) \\ \mathbf{B_c^T} &= \frac{1}{\alpha\tau}[1 \quad 1 \quad \dots \quad 1] \\ \mathbf{C^T} &= [\gamma_0 \quad \gamma_1 \quad \cdots \quad \gamma_{m-1}] \\ \mathbf{D} &= [K] \end{aligned} \tag{47}$$

In equation (13) we made a simplifying assumption that all input r_i are the same, however in general they need not be the same.

REFERENCES

1. Kasdin N. J. and Walter T. Discrete simulation of power law noise (for oscillator stability evaluation). In Proceedings of the 1992 IEEE Frequency Control Symposium, pages 274–283, 1992.
2. Chen X. Peng C. Huan H. Nian F. and Yang B. Measuring the Power Law Phase Noise of an RF Oscillator with a Novel Indirect Quantitative Scheme. Electronics, 8, 767:1 – 9, 2013.
3. Chorti A. and Brookes M. A Spectral Model for RF Oscillators With Power-Law Phase Noise. IEEE Transactions On Circuits and Systems-I: Regular Papers,, 53, 9:1989 – 1999, 2006.
4. Macucci M. and Marconcini P. Theoretical Comparison between the Flicker Noise Behavior of Graphene and of Ordinary Semiconductors. Journal of Sensors, 2020:11, 2020.
5. Matjelo N. J. and Khanyile N. Design, Implementation and Characterization of Helical Resonator for Ion Trapping Applications. International Research Journal of Modernization in Engineering Technology and Science. 3(05):1879 – 1888, 2021.
6. Matjelo N. J., Khanyile N., and Uys H. Design, Implementation and Characterization of RLC Resonator for Ion Trapping Application. International Research Journal of Modernization in Engineering Technology and Science. 3(05):1879 – 1888, 2021.
7. Matjelo N. J., Payne N., Rigby C. and Khanyile N. Demonstration of Rabi-Flops with Ytterbium 171 Trapped-Ion Qubits. International Journal of Scientific and Research Publications. 11(7):137 – 153, 2021.
8. Oliver W. D. Ball H. and Biercuk M. J. The role of master clock stability in quantum information processing. njp Quantum Information, 2, 16033:1 – 8, 2016.
9. arxiv:1304.7925 [cond-mat.mes-hall].
10. Falci G. D'Arrigo A. and Paladino E. Quantum Sensing 1/f Noise via Pulsed Control of a Two-Qubit Gate. In Proceedings 2019012029, pages 1 –8, 2019, 12, 29.
11. Rosenband T. et al. Alpha-dot or not: Comparison of two single atom optical clocks. Frequency Standards and Metrology, pages 20 – 33, October 05, 2008.
12. Physical review a 73, 031804(r) 2006.
13. Greenhall C. A. An approach to power-law phase-noise models through generalized functions. Metrolgia, 47:605 – 615, 2010.
14. arxiv:2008.00251.
15. Rev. mod. phys. 88, 041001 (2016).
16. Physical review a 93, 062511 (2016).
17. Nature physics,7 565, (2011).
18. Physical review a 89, 042329 (2014).
19. arxiv:astro-ph/0510081v3 9 jul 2008.
20. John A Davis, CA Greenhall, and PW Stacey. A kalman filter clock algorithm for use in the presence of flicker frequency modulation noise. Metrologia, 42(1):1, 2005.
21. Kumar A. Kumar R. and Kumar A. J. Effects of 1/f baseband noise and its suppression using kalman filter in ofdm system. International Journal of Engineering Research & Technology, 2:724 – 729, 2013.
22. Jarvis S. Barnes J. Efficient numerical and analog modeling of flicker noise processes. National Bureau of Standards Technical Note 604, 1971.
23. Matjelo N. J., Deconversion of Power-Law Noise to White Noise Through Direct and Indirect Model Inversion. International Journal of Innovative Science and Research Technology, 6(7): 287 - 290, 2021.

AUTHORS PROFILE

Naleli Jubert Matjelo, currently works as a lecturer at the National University of Lesotho (NUL). Obtained Bachelor of Engineering in Electronics degree at NUL in 2011, then MSc in Electrical Engineering degree at University of Cape Town in 2014 and lastly PhD in Physics at Stellenbosch University in 2020. Research interests include Control Systems, Computer Vision, Atomic & Laser Physics, Theoretical Physics, Econophysics and Quantum Finance. Publications available here: https://scholar.google.com/citations?hl=en&user=I_hyY2kAAAAJ

Sekhonyana Moeti, currently works as an instrument technician at Minopex Lesotho, which operates in Letseng Diamonds Mine. Obtained Bachelor of Engineering in Electronics degree at the National University of Lesotho in 2011, then MSc in Electrical Engineering degree at the University of Cape Town in 2015. Research interests include Measurement & Control Systems and Electrical/Electronics.

Molise Mokhomo, currently works as test automation lead at Mukuru in Cape Town, Wesstern Cape, South Africa. Obtained Bachelor of Engineering in Computer Systems & Networks degree at the National University of Lesotho in 2011, then MSc in Electrical Engineering degree at the University of Cape Town in 2014. Research interests include AI, Signal Processing, Software Engineering and Computer Vision.